NREL/TP-442-20281 • UC Category: 1211 • DE96000470

A Comparison of Baseline Aerodynamic Performance of Optimally-Twisted Versus Non-Twisted HAWT Blades

D. A. Simms
M. C. Robinson
M. M. Hand
L. J. Fingersh

Prepared for
Fifteenth ASME
Wind Energy Symposium
January 28-February 2, 1996

National Renewable Energy Laboratory
1617 Cole Boulevard
Golden, Colorado 80401-3393
A national laboratory of the U.S. Department of Energy
Managed by Midwest Research Institute
for the U.S. Department of Energy
under contract No. DE-AC36-83CH10093

Prepared under Task No. WE514430

Available to DOE and DOE contractors from:
Office of Scientific and Technical Information (OSTI)
P.O. Box 62
Oak Ridge, TN 37831
Prices available by calling (615) 576-8401

Available to the public from:
National Technical Information Service (NTIS)
U.S. Department of Commerce
5285 Port Royal Road
Springfield, VA 22161
(703) 487-4650

Printed on paper containing at least 50% wastepaper, including 10% postconsumer waste

Characterization and Comparison of Baseline Aerodynamic Performance of Optimally Twisted Versus Non-Twisted HAWT Blades

D. A. Simms
M. C. Robinson
M. M. Hand
L. J. Fingersh

National Renewable Energy Laboratory
Golden, CO 80401

ABSTRACT

NREL has completed the initial twisted blade field tests of the "Unsteady Aerodynamics Experiment." This test series continues systematic measurements of unsteady aerodynamic phenomena prevalent in stall-controlled horizontal axis wind turbines (HAWTs). The blade twist distribution optimizes power production at a single angle of attack along the span. Abrupt transitions into and out of stall are created due to rapid changes in inflow. Data from earlier experiments have been analyzed extensively to characterize the steady and unsteady response of untwisted blades. In this report, a characterization and comparison of the baseline aerodynamic performance of the twisted versus non-twisted blade sets will be presented for steady flow conditions.

BACKGROUND

This experiment uses a special three-bladed, downwind, 1-meter-diameter wind turbine. The rotor has 0.457-m (18 inch) constant-chord NREL S809 airfoils and operates at a fixed rotation rate of 72 RPM. The turbine, a modified Grumman Windstream 33, was extensively instrumented to provide accurate and detailed performance and test data (Butterfield et al., 1992) including; wind inflow, power production, aerodynamics, and structural response of the rotating blades and tower.

Previous and current turbine test configurations are shown in Figures 1 and 2, respectively. Constant-chord, twisted blades are used in the current test phase to explore the effects of twist on rotor aerodynamic performance. No other significant changes were made in turbine configuration.

Quantifying inflow behavior using a different meteorological tower configuration provided additional inflow data for the tests reported here. A vertical plane array of prop-vane anemometers situated in the prominent upwind direction was used in the previous phase. Multiple towers with cup anemometers and a hub-height sonic anemometer are used in the current phase. This was done to better characterize shear, and to provide local atmospheric stability measurements.

In both test configurations, one of the turbine blades was specially designed and instrumented to measure rotating aerodynamic forces. The instrumented blades were built identically, with approximately 150 surface-pressure taps connected by embedded stainless steel tubing to multi-channel differential pressure transducers located inside the blade. Resulting pressure data provide high-resolution aerodynamic lift and drag force measurements from the rotating airfoil. The pressure taps are located at four radial stations of 30%, 47%, 63%, and 80% span. There are 22 instrumented taps around the airfoil chord at each of these stations. Additional taps are located at various intermediate span locations. Other channels on the instrumented blade include four stations of both dynamic pressure and local flow angle. Pressure and local flow angle measurement locations are shown in Figure 3.

In order to collect large volumes of aerodynamic and force data from a rotating blade, an extensive instrumentation and data acquisition system development program was necessary (Fingersh, 1994). The resulting equipment provides highly accurate measurements in a rugged, rotating, field environment. Typical aerodynamic measurements include differential blade surface pressures over ±8300 N/m^2 (±1.2 psi) with an estimated measurement uncertainty of ±50 N/m^2 (±0.007 psi). Special equipment and computer-controlled calibration sequences are used to maintain required accuracy levels. A hub-mounted tripod boom can also be seen in Figures 1 and 2. Rotating data system electronics are housed in the enclosures on the inboard section of the hub boom.

Analog signals are filtered, sampled, and encoded into digital, pulse-code modulated (PCM), data streams. Both PCM and video signals are passed through slip rings and conducted down the tower to ground-based data processing computer systems. Data are archived to erasable-optical disk and CD-ROM media.

A video camera and lights are mounted on the outboard section. The camera focuses on the downwind suction side of the blade. There is also a camera mounted at the root of the instrumented blade that looks out along the blade span. The two video cameras can record the orientation of blade surface-mounted tufts and smoke distribution to help visualize the flow field.

Other rotating channels include blade flap and edge-bending moments, main-shaft bending and torsion, blade-tip acceleration, and pitch angles. A total of more than 180 channels on the rotor are simultaneously sampled at 520 Hz, or once per 0.83° of rotation. Non-rotating channels include turbine yaw position, yaw moment, tower bending, generator power, rotor RPM, and blade azimuth position. In the current test phase, upwind meteorological towers are instrumented to measure inflow wind velocity, wind direction, barometric pressure, and temperature. Horizontal wind shear, vertical wind shear, and boundary-layer stability are derived from the meteorological measurements.

DISCUSSION

In order to study how dynamic inflow conditions affect turbine aerodynamic performance, a baseline, or steady-state rotor response must first be established. Excursions from the baseline can then be explored to determine source phenomenology, and resulting effects on aerodynamic performance.

Unfortunately, steady conditions rarely occur in a field operating environment. Downwind HAWT geometries preclude the existence of true steady-state flow conditions because the turbine blades are always subjected to unsteady aerodynamic effects caused by passage though the tower shadow wake. Environmental phenomena including changing wind conditions, turbulence, wind shear across the rotor plane, and yaw error all contribute to unsteady perturbations. The resulting complex, stochastic environment under which turbines typically operate make it extremely difficult to quantify and characterize baseline turbine aerodynamic performance. Widely-varying aerodynamic responses are more the norm than the exception. These unsteady responses in turn exacerbate turbine structural dynamic responses and ultimately impact fatigue life.

Two dimensional (2-D) wind tunnel data are typically used to estimate steady-state wind turbine aerodynamic performance. Three-dimensional (3-D) effects inherent in the rotating environment alter 2-D rotor performance predictions and are independent of stochastic operating conditions. 3-D effects include tip losses and inboard stall delays due to rotation (Banks, 1963).

It is difficult to accurately ascertain baseline performance which includes 3-D effects. Baseline performance must be extracted from stochastic field turbine operating data. In this report, baseline conditions are defined as those in which the inflow exhibits "steady" conditions for three consecutive turbine cycles. This technique has proven useful in identifying baseline performance (Robinson, 1995). A cycle is defined as one complete rotation of the instrumented bladed starting from the top vertical position (0°). Data were scanned to search for those cycles where inflow velocities and yaw angles were well behaved within specified variance limits listed below. Mean values from these cycles are presented here as representative baseline operating conditions.

The large number of measurement channels and high data sample rates used in this experiment produce vast quantities of data. Each 10-minute data set requires approximately 300 MB of disk storage space. The untwisted data set consisted of 59 five-minute episodes, or a total of 20,557 blade cycles. The twisted data set consisted of six 10-minute episodes, or a total of 4320 blade cycles. Each 0.833 second rotor cycle contains over 100,000 data points. Each cycle from the entire data set for each test configuration was scanned for baseline conditions. Selection of each baseline data value resulted from examination of three consecutive rotor cycles exhibiting near-constant velocities at zero yaw error. The selection criteria included; 1) the standard deviation of the three cycle-averaged inflow wind velocities was less than 5% of the mean velocity; 2) the average yaw error for the three consecutive cycles was within ±1.5° for wind velocities less than or equal to 12 m/s, and ±5° for greater wind velocities; and 3) the yaw error standard deviation for the three consecutive cycles were less than 2.5°. The cycle-averaged value from the middle cycle was then used as the baseline. Fewer than 1% of the data cycles exhibited relatively steady baseline conditions under these criteria. These cycles, however, did provide sufficient information to establish the baseline power and angle of attack distributions reported here.

Measured angle of attack from a rotating airfoil, as shown in Figure 7, are somewhat difficult to obtain. Data values are based on local flow angle measurements from small counterbalanced flags located one chord length in front of the leading edge of the instrumented blade which self-align to the local flow direction. Each flag is mounted on a rotating shaft instrumented to determine angular position. Flag angle is measured relative to the blade aerodynamic chord line within an estimated uncertainty of ±1.0°. Actual angle of attack values are obtained by adjusting the local flow angle flag measurements with an upwash correction. The upwash correction (Figure 4) was obtained by testing an identically configured airfoil section and local flow angle flag in the CSU wind tunnel at Reynolds numbers of 300,000, 500,000, and 650,000, and at the Ohio State University wind tunnel at a Reynolds number of 1,050,000. Local flow angle flag measurements from the wind tunnel are shown on the abscissa in Figure 4, and geometric angle of attack (airfoil chord line relative to tunnel flow) on the ordinate. Each measured local flow angle value in the field test data set is multiplied by the upwash correction to obtain angle of attack. Resulting angle of attack values are estimated to be within an uncertainty of ±2° over the range of 0° to 40°. Other methods explored for use in determining angle of attack for these data sets are discussed in Shipley, et al., 1995.

An operating tip pitch angle of 3° was used for all twisted blade test data collected. The untwisted blade was operated at a fixed tip pitch angle of 12°. Blade twist distributions at these pitch settings are shown in Figure 5. These pitch settings stall-limited peak power production to within 20 kW. Pitch angle was set manually by the turbine operator at the start of each experiment. Pitch angle varied somewhat (±1.5°) during each data episode, as shown in Figure 6. The variations were caused by mechanical pitch linkage backlash which occurred in response to rotor aerodynamic loading.

Figure 7 compares baseline cycle-averaged aerodynamic performance of the untwisted and twisted blades at the 30%,

47%, 63%, and 80% span locations, respectively. Normal forces were obtained from integrated pressure values at each span location normalized by the local stagnation pressure. Estimated measurement uncertainties are ±0.05 for normal force and ±2.0° for angle of attack. Baseline measured data values are plotted as symbols with dotted lines showing trends. For comparison, the solid line shows 2-D data from Colorado State University (CSU) wind tunnel tests at a Reynolds number of 500,000.

From these figures, three different performance regimes are clearly established: 1) quasi-steady below static stall, 2) unsteady separated behavior above static stall, and 3) abnormally large normal force values at the inboard span location. Similar trends have been reported by Madsen, 1991 and Ronsten, 1992. The flow exhibits 2-D behavior outboard toward the tip. However, neither the twisted or untwisted blade results show significant differences (i.e. larger than the estimated measurement uncertainty) between baseline normal force coefficients.

Baseline cycle-averaged measured and predicted spanwise angle of attack distributions for the two turbine blade configurations are shown in Figures 8 and 9 for various inflow velocities. Predicted values identified by solid lines were obtained using the blade element momentum theory model PROP (Tangler, 1983). As expected, PROP results shown in Figure 8 predict considerable angle of attack variation along the span of the untwisted blade. At a typical 12 m/s inflow velocity, angle of attack ranged from 35° at the 30% span location to 10° at the 80% span location. Three cycle-averaged measured values are shown for each span location, and measured data trends are shown with dotted lines. Measured angle of attack values differ somewhat, however, especially in mid-span locations at higher angles of attack. For example, the difference between predicted and measured angle of attack at 13.5 m/s and 63% span is in excess of 15°. The authors suspect that these differences are caused by stall hysteresis-induced flow perturbations as they occur in regions of the blade where delayed stall is evident.

PROP was used to design the twisted blade for optimized rotor power production at a constant angle of attack along the full span. This design criteria is more typical of standard industry turbines. Another objective was to try to produce abrupt transitions into and out of stall across as much of the blade span as possible. It was hoped that variations in wind speed, or transitions through the tower wake, would produce dynamic stall-induced structural and audible impulses. As shown in Figure 9, full-span stall transition is predicted to start at an inflow velocity of approximately 12 m/s*. During field operation, no obvious abrupt stall-related effects have been seen. Measured angle of attack values (Figure 9) are significantly different than predicted. Variability between baseline cycle-averaged measured angle of attack values for the twisted blade is much greater than the untwisted blade. This variability tends to increase inboard. At a velocity of 13.5 m/s, baseline angle of attack at the 47% span location varies by 5°. The offset between the measured and predicted curves are also more significant. At 13.5 m/s and 30% span, these differ by as much as 7°.

*The 2-D wind-tunnel leading edge separation for the S809 occurs at ~17°. Operating at a tip pitch angle of -7° flattens out the curve and optimum stall conditions are predicted to occur at 8 m/s.

FUTURE WORK

Now that the baseline operating conditions for the untwisted and twisted rotor configurations have been determined, work will begin on isolating how various turbine operating conditions affect resulting aerodynamic performance. The experiment data sets will be searched to extract "steady" cycles of specific operating conditions. The effects of yaw error, horizontal wind shear, vertical wind shear, and atmospheric stability will be evaluated. Cycles will be extracted in which yaw errors are ±15° and ±30° while shear is zero and stability is neutral. Cycles will also be extracted under specific levels of horizontal shear, while vertical shear and yaw are zero, and stability is neutral. Similarly, the data set will be searched for cycles which have specific values of vertical shear, while horizontal shear and yaw error are zero, and stability is neutral. Finally, data sets will be searched for operating conditions during four levels of atmospheric stability: stable, critically stable, neutral, and unstable; during which yaw and shear are zero.

CONCLUSIONS

Field tests of both an untwisted and twisted rotor blade package have documented the extremely complex and stochastic environment in which wind turbines must operate. In order to establish the "baseline" performance characteristics of both geometries, aerodynamic data were cycle-averaged and sorted under inflow conditions with very stringent mean variance tolerances. The resulting aerodynamic normal force versus angle of attack data indicated three regions of unique performance where:

- Below static stall, airfoil sections along the blade span exhibited 2-D behavior,
- Near 2-D stall, airfoil sections did not exhibit the character normal force drop-off with increasing angle of attack, and normal force distributions remained flat through 40°, and
- At inboard span locations, normal force increased near monotonously with angle of attack, well in excess of 2-D behavior.

Little, if any, difference in cycle-averaged performance was observed between the twisted and untwisted blade geometries. The same three distinct performance regions, identified previously by these authors, exist for both geometries.

The measured angle of attack along the span deviated substantially from predicted values using the PROP design code. The source for this deviation is under investigation. One consequence is that measured angle of attack values on the untwisted rotor can be considerably different than predicted, especially at intermediate span locations, with variations up to 10° evident. This may result in a blade that is less dynamically active than originally desired, however, instantaneous and unsteady performance indices of the twisted blade geometry have yet to be quantified.

REFERENCES

Banks, W. H. H., and Gadd, G. E., 1963, "Delaying Effect of Rotation on Laminar Separations," AIAA Journal, Vol. 1, pp. 941-942.

Butterfield, C. P., Musial, W. P., Simms, D. A., 1992, "Combined Experiment Phase I Final Report," National Renewable Energy Laboratory, Golden, Colorado, NREL/TP-257-4655.

Fingersh, L. J., Simms, D. A., Butterfield, C. P., Jenks, M. D., 1995, "An Overview of the Unsteady Aerodynamics Experiment Phase III Data Acquisition System and Instrumentation," American Society of Mechanical Engineers, *Proceeding of ASME 1995 Wind Energy Conference*, Vol. 16, Houston, Texas, pp. 277-280.

Madsen, H. A., 1991. "Aerodynamics of a Horizontal-Axis Wind Turbine in Natural Conditions," Riso National Laboratory, Roskilde, Denmark, Riso-M-2903.

Robinson, M. C., Galbraith, R. A. McD., Shipley, D. E., Miller, M. S., 1995, "Unsteady Aerodynamics of Wind Turbines," AIAA 95-0526, 33rd Aerospace Sciences Meeting and Exhibit, Reno, NV.

Ronsten, G., 1992, "Static Pressure Measurements on a Rotating and Non-rotating 2.375 m Wind Turbine Blade. Comparison with 2-D Calculations," Journal of Wind Engineering and Industrial Aerodynamics, Vol. 39, pp. 105-118.

Shipley, D. E., Miller, M. S., Robinson, M. C., Luttges, M. W., Simms, D. A., 1995, "Techniques for the Determination of Local Dynamic Pressure and Angle of Attack on a Horizontal Axis Wind Turbine," National Renewable Energy Laboratory, Golden, Colorado, NREL/TP-442-7393.

Tangler, J., 1983, "Horizontal-Axis Wind System Rotor Performance Model Comparison - A Compendium", RFP-3508, UC-60.

ACKNOWLEDGMENTS

This work was sponsored by the U.S. Department of Energy under contract number DE-AC36-83CH10093. The authors wish to thank Derek Shipley and Dave Jager for preparing some of the drawings used in this report.

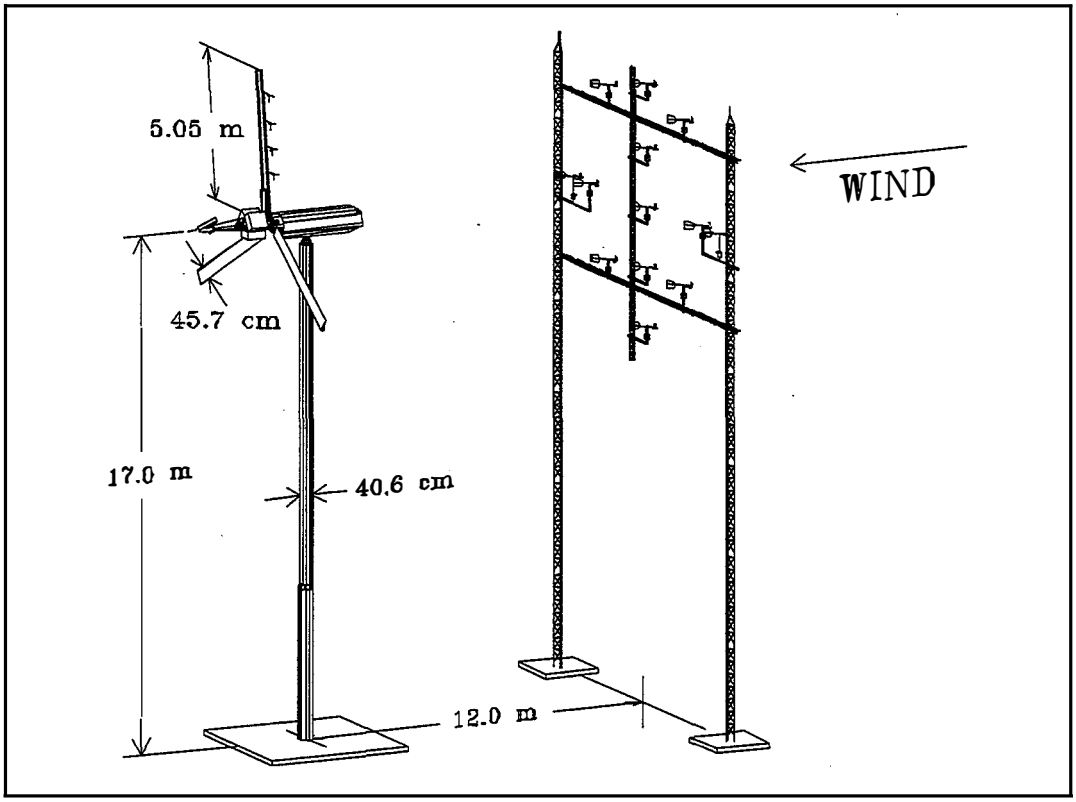

Figure 1. Untwisted blade test configuration.

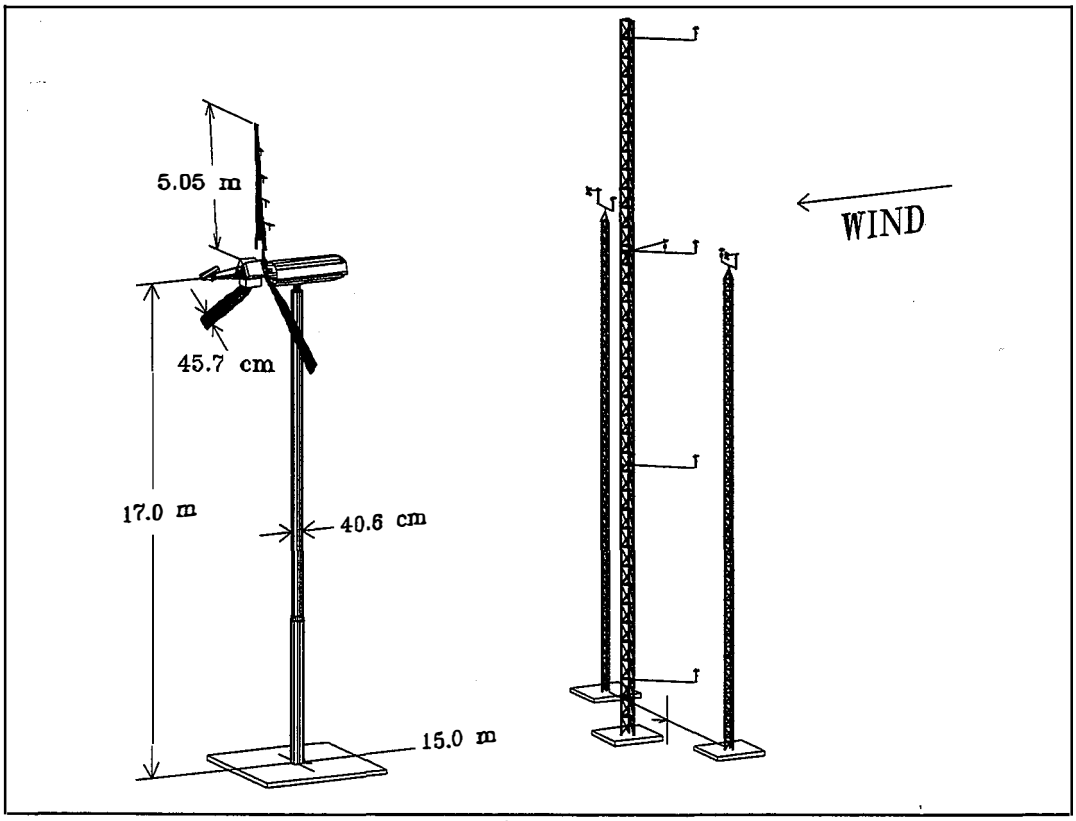

Figure 2. Twisted blade test configuration.

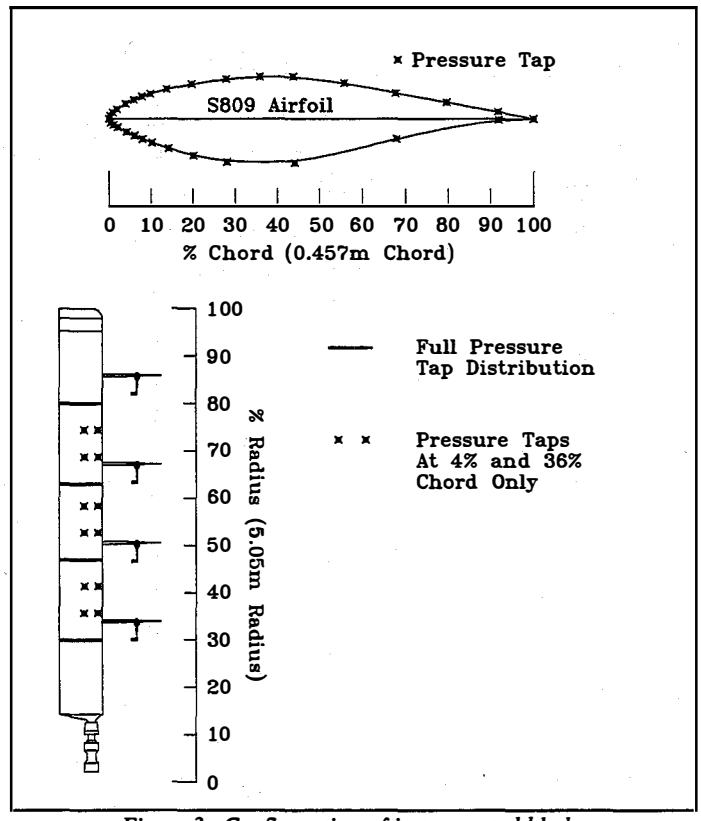

Figure 3. Configuration of instrumented blade.

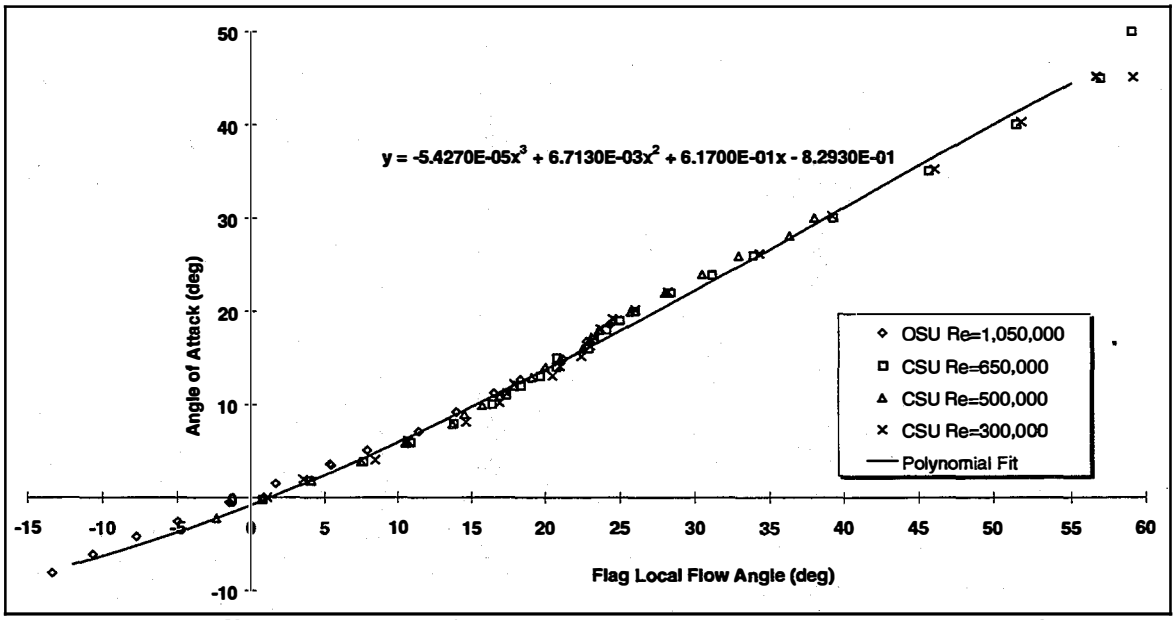

Figure 4. Upwash correction used to convert local flow angle measurements to angle of attack.

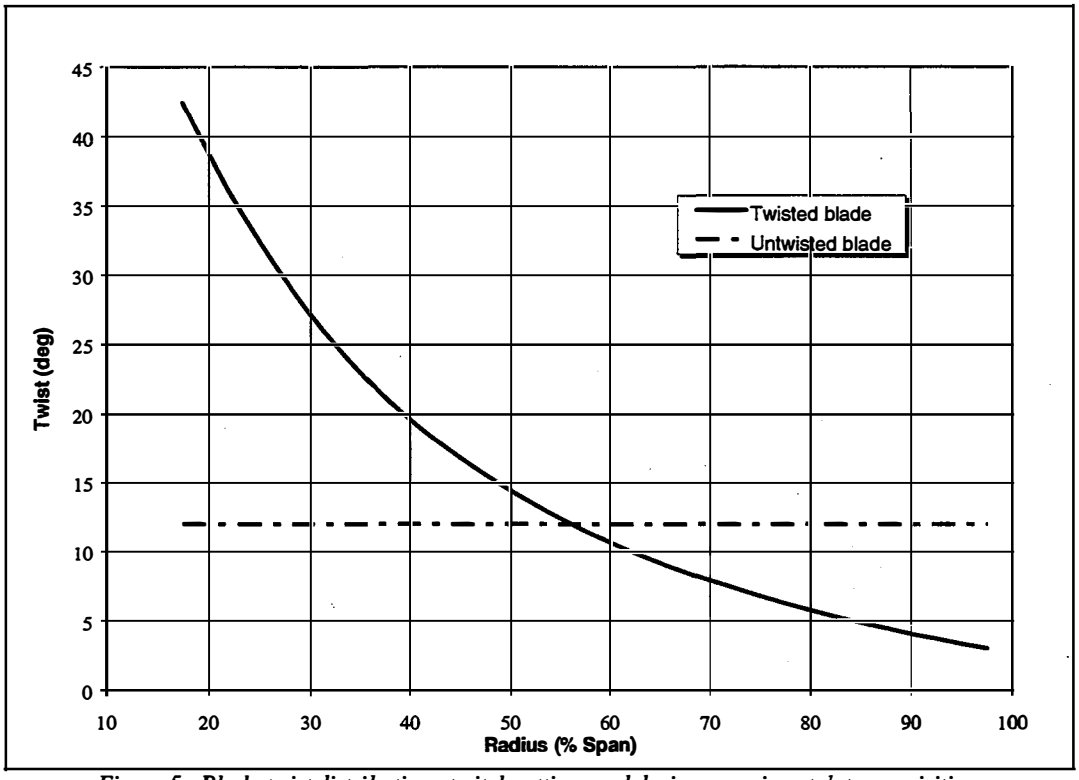

Figure 5. Blade twist distribution at pitch setting used during experiment data acquisition.

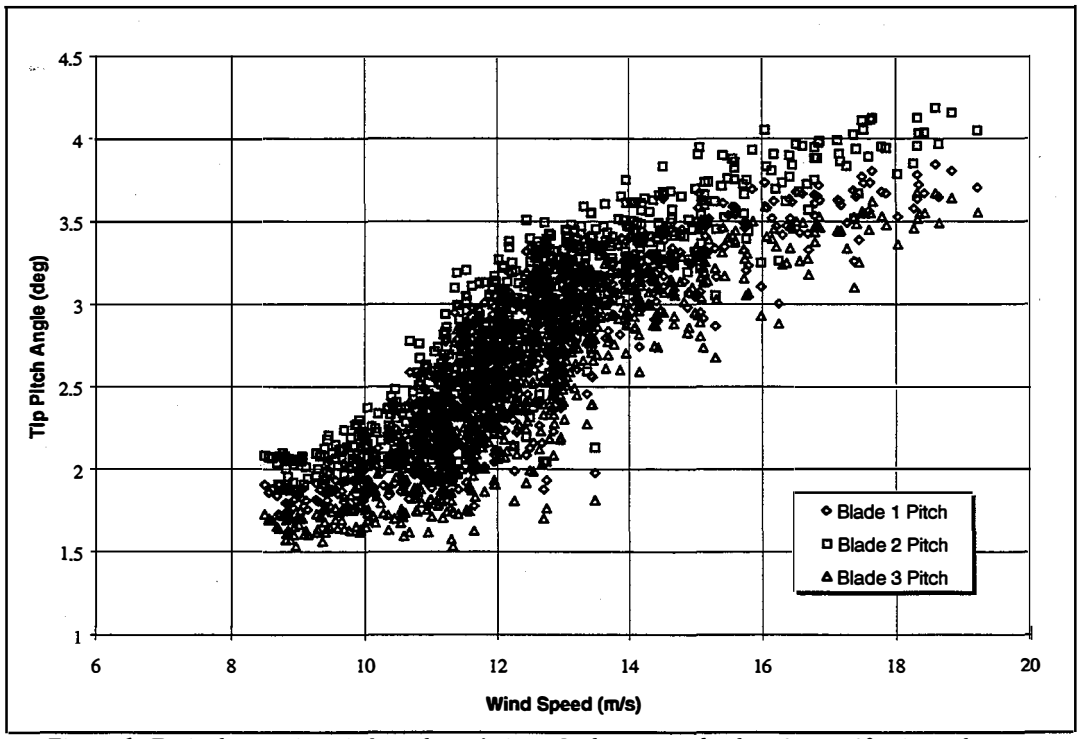

Figure 6. Typical operating pitch angle variation. Cycle-averaged values from a 10-minute data set.

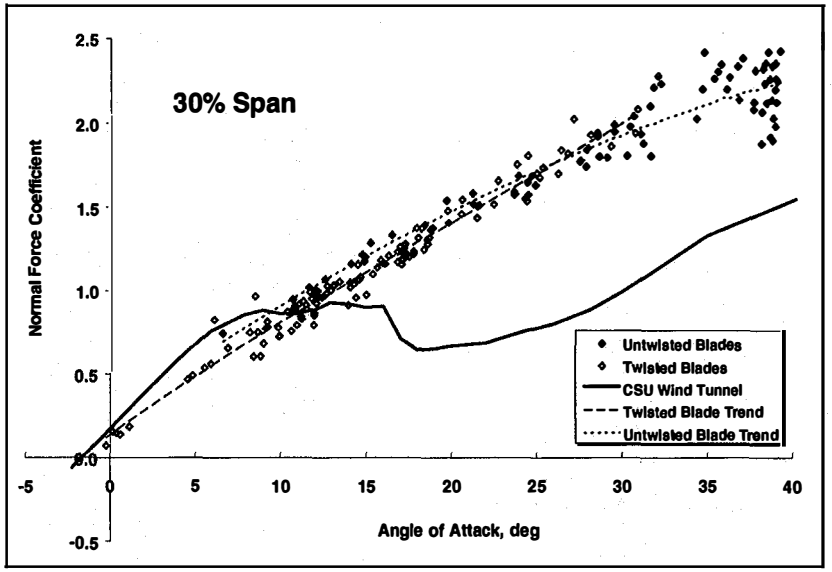

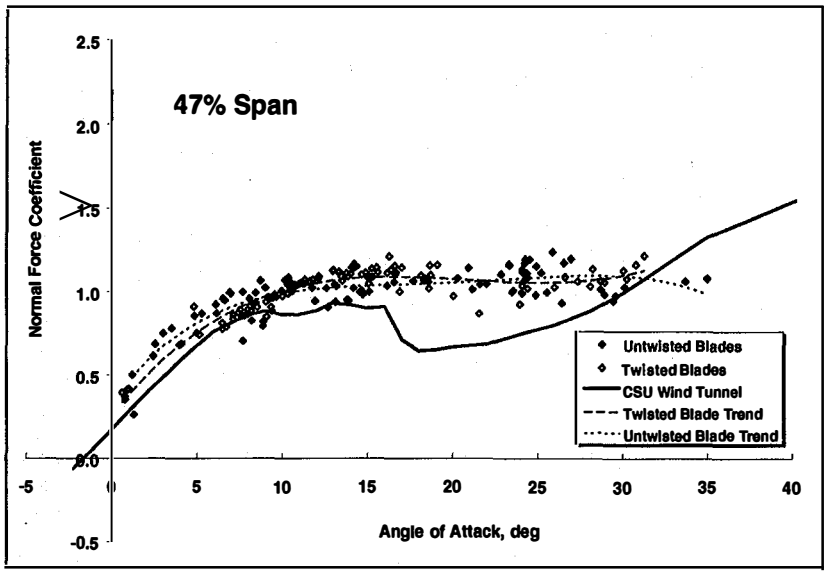

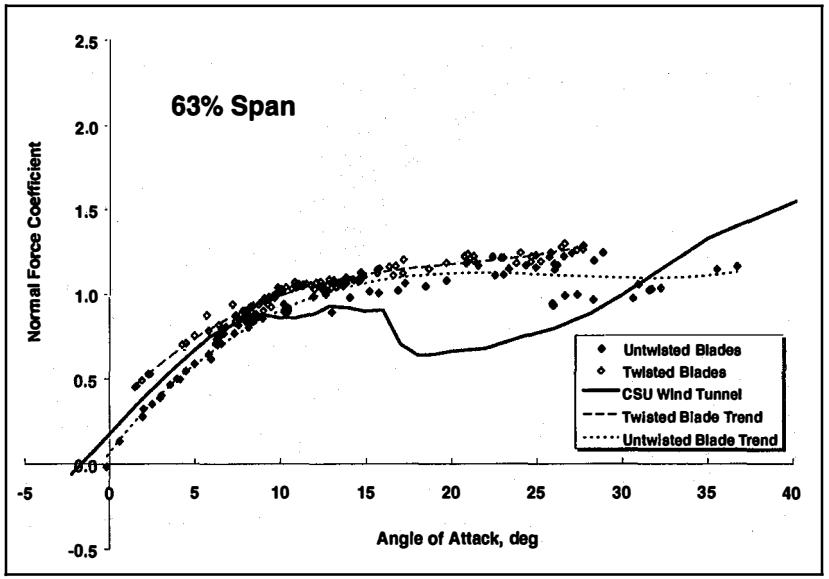

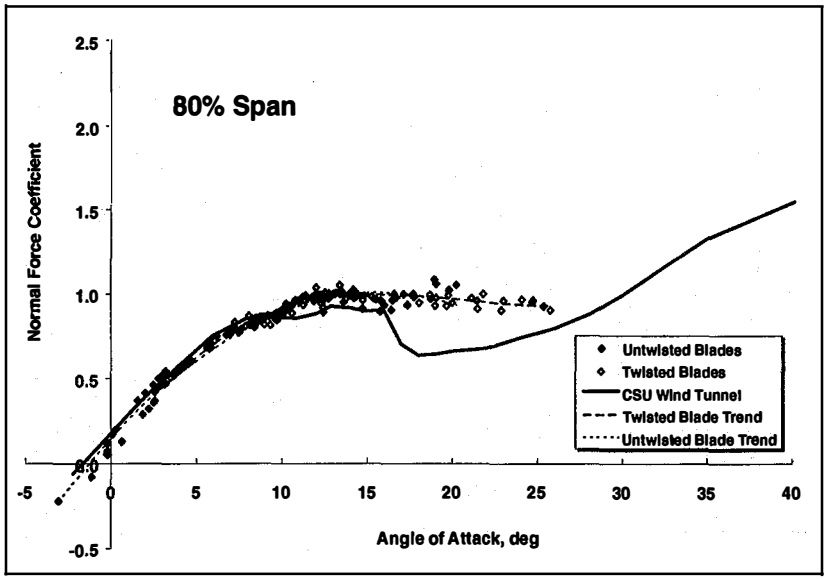

Figure 7. Baseline cycle-averaged twisted and untwisted blade normal force vs. angle of attack at the 30%, 47%, 63%, and 80% span locations.

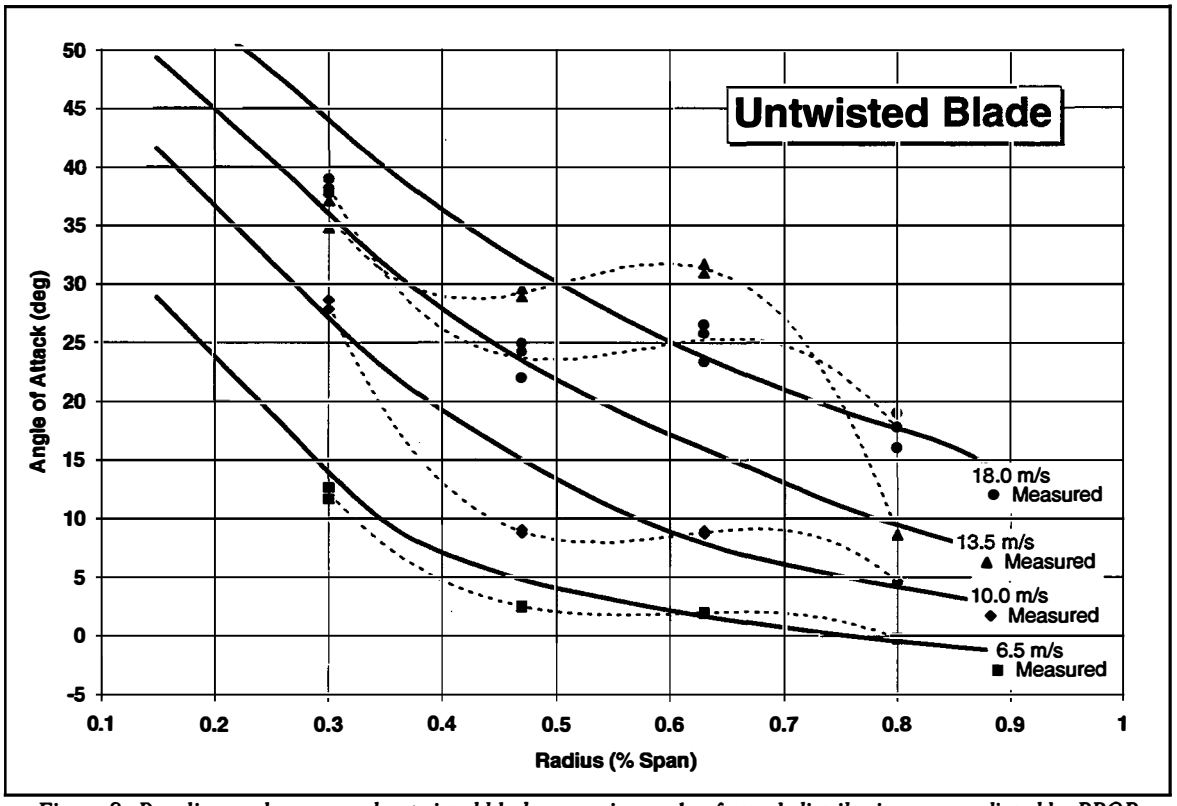

Figure 8. Baseline cycle-averaged untwisted blade spanwise angle of attack distributions as predicted by PROP compared with measured angle of attack distributions (corrected for upwash).

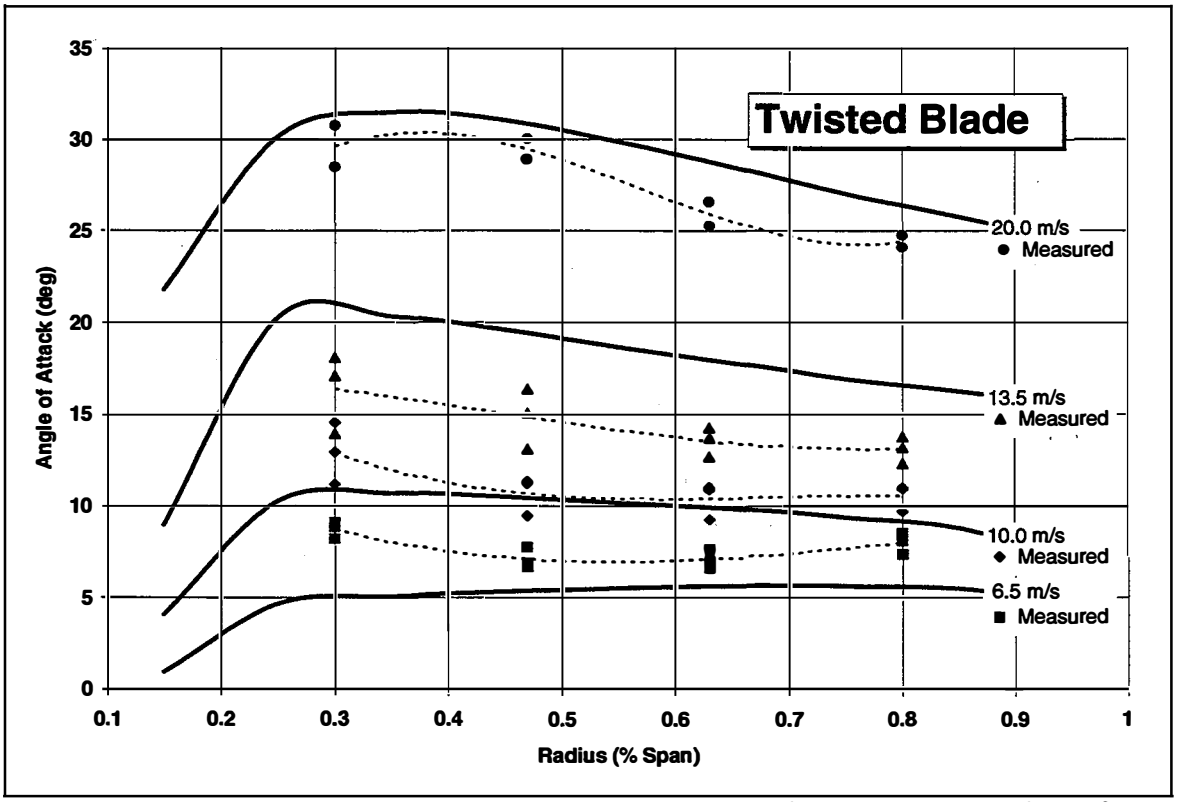

Figure 9. Baseline cycle-averaged twisted blade spanwise angle of attack distributions as predicted by PROP compared with measured angle of attack distributions (corrected for upwash).